

Hybrid-Attention Guided Network with Multiple Resolution Features for Person Re-Identification

Guoqing Zhang, *Member, IEEE*, Junchuan Yang, Yuhui Zheng, Yi Wu, and Shengyong Chen *Senior Member, IEEE*

Abstract—Extracting effective and discriminative features is very important for addressing the challenging person re-identification (re-ID) task. Prevailing deep convolutional neural networks (CNNs) usually use high-level features for identifying pedestrian. However, some essential spatial information resided in low-level features such as shape, texture and color will be lost when learning the high-level features, due to extensive padding and pooling operations in the training stage. In addition, most existing person re-ID methods are mainly based on hand-craft bounding boxes where images are precisely aligned. It is unrealistic in practical applications, since the exploited object detection algorithms often produce inaccurate bounding boxes. This will inevitably degrade the performance of existing algorithms. To address these problems, we put forward a novel person re-ID model that fuses high- and low-level embeddings to reduce the information loss caused in learning high-level features. Then we divide the fused embedding into several parts and reconnect them to obtain the global feature and more significant local features, so as to alleviate the affect caused by the inaccurate bounding boxes. In addition, we also introduce the spatial and channel attention mechanisms in our model, which aims to mine more discriminative features related to the target. Finally, we reconstruct the feature extractor to ensure that our model can obtain more richer and robust features. Extensive experiments display the superiority of our approach compared with existing approaches. Our code is available at <https://github.com/libraflower/MutipleFeature-for-PRID>.

Index Terms—Person re-identification, multiple scale and multiple resolution features, attention mechanism.

I. INTRODUCTION

Given a query image of a pedestrian, re-identification (re-ID) is to identify the person from a different cameras without overlapping fields of view. Due to complicated and variable conditions such as person posture, camera view, and low resolution, person re-ID still encounters great challenges. Currently, existing person re-ID approaches mainly contains two aspects: traditional algorithms and deep learning-based algorithms. Most traditional person re-ID approaches are mainly based on hand-craft features, which cannot adapt well to complex scenarios with a large amount of data. Recently, numerous deep learning based algorithms have been



Fig. 1. (a) The two images on the left represent two different images of the same person whose bounding boxes do not match perfectly. (b) The two images on the right show the activation map of our method. It can be seen that our method can still find more discriminative local regions (inside the red border) completely.

presented and greatly improved re-ID performance. Different from traditional methods, deep learning approaches can extract highly discriminative image features and learn more accurate similarity measurements.

Although deep learning based person re-ID algorithms have received increasing explorations [8], [21], [33], [38], [51], it is still very difficult to effectively apply them to real scenes. Prevailing algorithms are usually designed based on the manually annotated datasets, which provide accurate pedestrian detection bounding boxes. However, in practice, the fuzzy and misaligned bounding boxes, detected automatically often appear and seriously degrade the performance of existing algorithms (as shown in Figure 1 (a)). In addition, due to some limitations of the deep models, some discriminative features will be lost with the deepening of the network, it is difficult to apply them in practice.

To match the person identity, features extracted from the top (deep) layer of training network are generally used for the similarity matching. However, since one deep neural network usually contains multiple feature extraction layers, which are superimposed layer by layer. From the shallow to the deep layer, the visual concepts captured by feature mapping tend to be more abstract and the semantic levels are higher, i.e., features of the last layer of a network mostly encode semantic information, like object presence [29], may lose some basic information, such as the color of clothes or the shape of humans body. To remedy this problem, we should reason simultaneously across multiple levels of semantic abstraction. That means both deep features and shallow features of a CNN should be considered jointly.

G. Zhang is with the School of Computer and Software, Nanjing University of Information Science and Technology, China, 210044 (e-mail: guoqingzhang@nuist.edu.cn).

J. Yang and Y. Zheng are with the School of Computer and Software, Nanjing University of Information Science and Technology, 210044, China (e-mail: chuenhot@hotmail.com; zheng_yuhui@nuist.edu.cn), (Corresponding author: Yuhui Zheng, Shengyong Chen).

Y. Wu is with the Wormpex AI Research (e-mail: ywu.china@gmail.com)

S. Chen is with the School of Computer Science and Engineering, Tianjin University of Technology, Tianjin 300384, China (e-mail: sy@ieee.org)

Part-based models have shown superior performance in many computer vision tasks because of their robustness to image occlusion or partial variation challenges. Actually, the performance of person re-ID is also affected by these challenges. Part-based Convolutional Baseline (PCB) structure [38] is a simple and effective model, which is one of the most acknowledged part-based approaches, and its performance exceeds most deep learning models. However, the current PCB model has some shortcomings: (1) PCB structure only considers the divided features and completely ignores the role of global features in the whole network; (2) The PCB structure ignores the incomplete image detection and blurred bounding boxes in real scenes.

Recently, many researchers have introduced attention mechanisms into deep models to strengthen the learned features and suppress some disturbances of the features [17], [50], [55], [56]. The purpose of attention is to focus on important features and ignore irrelevant features. This is consistent with the task of person re-ID. For judging whether a feature is important, it is necessary to weigh it within the scope of global features.

Motivated by these concerns, we proposed a hybrid-attention guided network with multiple resolution features for person re-ID, which aims to enhance the representation capacity of the CNN models to discriminatively learn the pedestrian features. The framework is shown in Figure 2. Since some important clues will be lost in the process of learning high-level features, we fuse the deep and shallow network features to eliminate the influence of the disappearance of some features in our network. Then the fused embeddings can be divided into several parts and we connect them to obtain global and local feature to alleviate the affect caused by the misaligned bounding boxes. In addition, we also introduce two different attention mechanisms, i.e., spatial and channel attention mechanisms, to mine the most informative parts of feature embeddings that are related to our target. The spatial attention is used to explore where the significant feature is. The channel attention is used to explore what noteworthy element in the feature is. Through the joint action of two kinds of attention mechanisms, we can increase the discriminability of features extracted by our model. Extensive experiments present the superiority of our model on four large datasets.

II. RELATED WORK

A. Deep Learning for Person Re-ID

Person re-ID is usually regarded as a sub-problem of image retrieval [18]. It refers to the task of finding the target in different time periods of videos captured from different cameras in different locations under the condition of a given pedestrian. Traditional person re-ID approaches are mainly focused on learning better manual visual features to reduce intra-person divergence and enhance the inter-person discrimination capability [1], [4], [6] or designing appropriate distance metric to accurately measures the similarity of different identities [2], [3], [5], [7]. In recent years, with the extensive progress of deep learning technology, it has been widely adopted to person re-ID tasks [9], [10], [12], [11], [13], [16]. Different from traditional re-ID approaches, methods based on deep learning

can adaptively learn discriminative features from pedestrian images [11], [17], [43] and contribute a lot to the re-ID task.

Previous person re-ID methods use global features of the whole image to match images [21], [22], [25], [41], which ignore various partial information of a given person. Recently, researchers found that local features show a great prospect for dealing with the misalignment of the pedestrian images. Therefore, extracting various local features from a large-scale dataset to improve re-ID performance is now the new mainstream [14], [16], [17], [24], [10], [11]. The idea of extracting in different solutions at multiple stages and using skip connections to combine multiple stage features has proven to be very useful in the field of target detection [31], [32], image classification and object recognition. This idea has also been exploited in person re-ID and promoted re-ID model to obtain very accurate prediction result [39], [40]. However, previous person re-ID methods usually pool the features of different stages into a single vector, which will inevitably lose some feature information of different stages [33]. Therefore to reduce this loss, we keep the size of feature maps from previous stages the same as that of the last stage.

B. Local Features for Person Re-ID

Global features and local features extracted by CNNs are widely used to perform person matching. The global feature allows the network to extract feature from the whole image without considering all local information [44], [33]. Due to the complexity of pedestrian images, a single global feature cannot meet the performance requirement, so learning more complex local features has become a research hotspot [16], [17], [24], [28], [29].

Feature map partition is a very common feature extraction algorithm [24], [38], [15], [13]. Most of the current methods adopt integrated global features and many stripe-based features to achieve advanced performance by linear pooling the partitioned feature maps [16], [26], [30], [66]. In [63], a multi-level network was proposed to decompose human features into multiple fine-grained local features, and fine-grained local features of different levels were integrated at the end of the model. Tay et al. [17] used three independent structures to obtain local features, global features and pose features, respectively, and then fused these three kinds of information to obtain final feature.

C. Attention Mechanism for Person Re-ID

Attention mechanism has been widely used in a variety of deep learning domains, such as image processing, natural language processing, speech recognition and so on. The human visual system tends to pay attention to some information of assist judgment in the image and ignore the irrelevant information. Therefore, in computer vision community some parts of the input may be more useful to the target task than others. The attention mechanism allows the model to adaptively focus on certain parts of the input related to the target.

Attention mechanism has also been adopted to address the re-ID task [17], [56], [55], [58], [45], [38], [50]. Many models

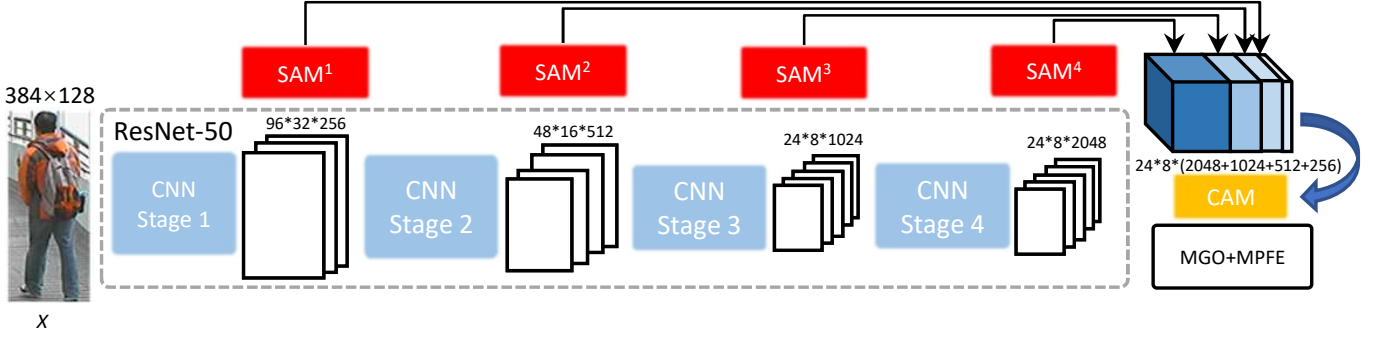


Fig. 2. Architecture of our model for person re-ID. Our proposed model consists of ResNet-50, SAM, CAM, MGO and MPFE. We extracted features from different stages of the network (ResNet-50), weighted them through the spatial attention module (SAM), spliced them together by channels, and then weighted the spliced feature maps through the channel attention module (CAM), followed by multi-granularity feature extraction (MGO+MPFE).

hope to find out more discriminative features (color or texture) in the image through attention mechanism, and ignore the other features (background) which are irrelevant to task. Sun et al. [27] simply used the attention mechanism to locate the visible areas in a given image through a positioning method and learned their local features based on these visible areas.

III. THE PROPOSED METHOD

Previous person Re-ID methods usually adopted the highest-level features for representing pedestrian, such as the output of the last convolutional layer of Resnet-50. Although it is very useful in representing object images using high-level features, yet at the same time some low-level features such as texture and color information will be lost. These low-level features are very significant clues for performing person re-ID. More importantly, in the last several layers of neural network, the distinguishing rate of feature map is lower, which may not accurately represent the patterns on clothes, facial subtle features and differences in posture and other details. This indicates that person re-ID methods benefit from information fusion with multiple layers.

A. Fusion of Multiple Resolutions

The Fusion of Multiple Resolution (FMR) module is mainly composed of the backbone network, which is realized by fusing the features of different layers of the backbone network. As shown in Figure 2, we will fuse features at different stages in the network. Since the feature maps of the previous stages are usually large, we keep the size of feature map output from each stage the same through the operation of Max pool, so as to ensure that the features of different stages can be spliced in the fusion stage.

Before and after splicing, we will carry out attention weighting on the feature map, expecting to learn more significant features through the network.

B. Hybrid-Attention Mechanism

Hybrid-Attention Mechanism(HAM) contains two modules: Spatial Attention Module (SAM) and Channel Attention Module (CAM) [64]. Because our features are obtained by fusing different resolutions of features, we expect to mine features

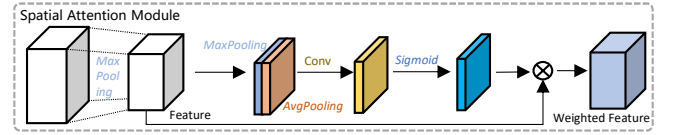


Fig. 3. Pipeline of Spatial Attention Module (SAM).

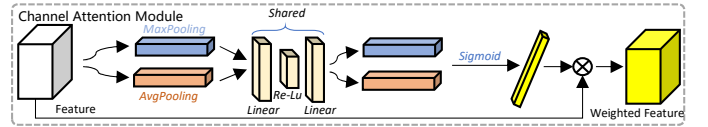


Fig. 4. Pipeline of Channel Attention Module (CAM).

with strong semantic expression in spatial dimension by using SAM. Since the connection operation expands the dimension of channels after feature fusion, as a result the relevance and importance of different channels can be explored by using CAM.

Spatial Attention Module (SAM). We exploit the relationship of feature space to generate spatial attention map. SAM mainly focuses on ‘where’ the significant part of the feature is. We first use average pooling and maximum pooling to obtain two different kinds of information of features, and connect them according to channels as the initial effective features of our spatial attention. Then our final spatial attention map can be generated by using convolution operations and sigmoid function. Details of the operation are described below.

The pipeline of SAM is shown in Figure 3, by using two different pooling operations, two two-dimensional features from the original features can be generated, denoted as F_{max}^{SAM} and F_{avg}^{SAM} . Then we connect these two features and generate the final two-dimensional spatial attention map by using the convolution operation and sigmoid function. Thus, the finally spatio-temporal attention can be defined as:

$$\begin{aligned} M_{SAM}(F) &= \sigma(f([AvgPool(F); MaxPool(F)])) \\ &= \sigma(f([F_{max}^{SAM}; F_{avg}^{SAM}])) \end{aligned} \quad (1)$$

where σ is the sigmoid function and f means the convolution layer.

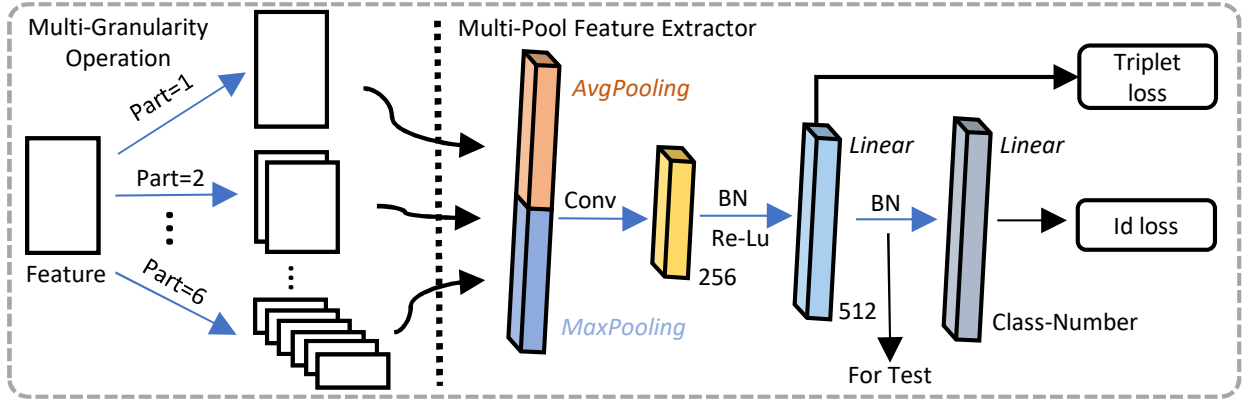


Fig. 5. Illustration of multi-granularity operation (MGO) and multi-pool feature extractor (MPFE). The MGO module is responsible for partitioning embeddings to obtain different granularity of local features. The MPFE module is used to extract the final feature.

Channel Attention Module (CAM). The channel attention map can be generated through the inter-channel relationships of features. Since the connection operation expands the dimension of channels after the feature fusion, we need to weight each channel to find the channels that are helpful to identify person's ID. Since each channel of the feature map is considered to be a feature detector, it is mainly concerned with what the noteworthy content in the input image for the channel attention is. In order to get the channel attention map, we also use maximum pooling and average pooling to obtain different types of information in the feature map.

As shown in Figure 4, we first get different information of the channels through the operations of maximum pooling and average pooling, denoted as F_{max}^{CAM} and F_{avg}^{CAM} . And then we obtain the channel attention map through a shared multi-layer linear operation, which includes two linear layers and Re-Lu activation functions. Later, the final channel attention map can be obtained by adding these two kinds of information. The final attention calculation can be briefly expressed as:

$$\begin{aligned} M_{CAM}(F) &= \sigma(f_{multi}([AvgPool(F) + MaxPool(F)])) \\ &= \sigma(f_{multi}([F_{avg}^{CAM} + F_{max}^{CAM}])) \end{aligned} \quad (2)$$

where σ represents the sigmoid function and f_{multi} represents the shared multi-layer linear.

C. Multi-Granularity Operation

Multi-Granularity Operation (MGO) module aims to obtain local features from feature map. We set the number of block levels as k , and each level will get different granularity of local features.

We first obtain feature $F \in R(C * H/k * W)$ according to the fusion and attention operations (as shown in Figure 2). Since the number of block levels is set as k , we can obtain k local features $F_{1 \sim k} \in R(C * H/k * W)$. Then, splicing these k local features according to different levels to get different granularity of local features. We set k as 6 and $part \in [1, k]$; When $part = 1$, the obtained feature is $F \in R(C * H * W)$; When $part = 2$, two local features can be obtained, denoted as $F_1 \in R(C * H_{1 \sim k-1} * W)$ and $F_2 \in R(C * H_{2 \sim k} * W)$, respectively; Similarly, when $part = 6$, the obtained six local

features can be expressed as $F_k \in R(C * H_k * W)$, where $k \in [1, 6]$.

Through multi-granularity operation, different granularity of local features can be obtained. We further adopt multi-pool feature extractor on these local features to obtain the final feature.

D. Multi-Pool Feature Extractor

After multi-granularity operation, features will be inputted into Multi-Pool Feature Extractor. Most existing feature extractors only use global average pooling as the initial step of feature extraction to obtain the final feature. However, maximum pooling is also an important way for collecting object feature, which can be used as a feature extraction strategy together with average pooling. Therefore, the maximum pooling and average pooling are simultaneous used in our feature extractor.

As shown in Figure 5, we can get two feature vectors by adopting the maximum pooling and average pooling for the obtained feature map, and then splicing the two parts. As the dimension increases after splicing, the time complexity will also increase greatly, a $1 * 1$ convolutional layer is introduced to reduce the dimension of the feature. After batch norm (BN) layer and Re-Lu activation function, the dimension of feature is changed into 512-dimensional through a linear layer, and the reduced feature is used to calculate the triplet loss. Then, the final classification features can be obtained through a BN layer and a linear layer, which are used to calculate ID loss.

E. Multiple Loss Function

In order to learn discriminant features, two different loss functions, including ID loss [4] and triplet loss [23] are exploited in our network.

Identification loss: In general, ID loss is defined as:

$$\begin{aligned} L^{id} &= \frac{1}{N_{id}} \sum_i \sum_{k,l} s \left((W_c^{k,l})^T x_i(l, k) \right) \\ &= \frac{1}{N_{id}} \sum_i \sum_{k,l} -\log \frac{(w_c^{k,l})^T x_i(l, k)}{\sum_j (w_j^{k,l})^T x_i(l, k)}, \end{aligned} \quad (3)$$

where N_{id} is the size of training images, $W_c^{k,l}$ represents the output of the fully connection layer, s represents the softmax function and c is the ID of the input image I_i .

Triplet loss: Given three samples I , I_p and I_n , where I_p is a true matching of I , while I_n is a wrong matching of I . The goal of triplet loss is to find a new feature space such that in this space, sample I and I_p have a much smaller distance than the distance between sample I and I_n . The triplet loss is expressed as

$$L^{tp} = \frac{1}{N_{tp}} \sum_{I, I_p, I_n} [d(f(I), f(I_p)) - d(f(I), f(I_n)) + \delta]_+, \quad (4)$$

where δ is the super parameter for representing the interval, which aims to control the distance between samples; $[\cdot]_+ = \max(\cdot, 0)$ represents the hinge loss function and N_{tp} represents the number of available triplets.

Therefore, we define the total loss of our network as:

$$L^{all} = \frac{1}{N} L^{id} + \frac{1}{M} L^{tp} \quad (5)$$

where N represents the number of ID losses calculated, and M represents the number of triplet losses.

F. Bag of tricks

Random Erasing. Due to the limitation of person bounding boxes, pedestrians usually lie in the same position and occupy the most image areas. Thereby, random erasing strategy is used in person re-ID task. Since pedestrians can be blocked at any positions in practical scene, we randomly select the rectangular area on the whole image and erase it. In the training stage, the random erasing will be performed with a certain probability. For images in one batch, assume that P is the probability of random erasing, $1-P$ is the probability of pedestrian images remaining unchanged. Then the random erasing will randomly select a point in the image and remove a rectangular region with this point as the center, where the size of this region is randomly selected within an interval. Finally, the training images with different occlusion levels can be generated during this process.

Warm-up Learning Rate. The performance of person re-ID model is easily affected by learning rate. At the beginning of training, we random initialize the weights of the model. If we select a relatively large learning rate, it may result in model shake. However, if we adopt warm-up learning rate, the learning rate within the first few epochs can be reduced. Using such a small learning rate, the model can gradually tend to be stable. When the model is becoming relatively stable, the pre-set learning rate can be selected for training, which can make the model converge faster and have a better effect.

Label Smoothing with ID loss. In existing deep learning models, the final feature is usually a one-dimensional vector, and person re-ID is considered as a classification problem. As for the loss function, we need to fit the real probability by using the predicted probability. However, such a fitting result cannot guarantee the generalization ability of the model, which is easy to cause overfitting. We can use label smoothing to alleviate this problem.



Fig. 6. Exemplary images in Market-1501, DukeMTMC-reID, MSMT17 and CUHK03 datasets. Each column represents the images of same person from different cameras.

IV. EXPERIMENTS

To verify the superiority of our model, four datasets such as Market-1501[34], DukeMTMC-reID[19], CUHK03[35] and MSMT17[65] are used in our experiments.

A. Experimental Setting

Implementation details: To obtain more detailed information from person images, following the experiment setting in [38], all images of input are resized to 384×128 . In our model, we utilize the ResNet-50 network with the pretrained weights on ImageNet as the backbone network. We remove the last full connection layer and bottom sampling in the last part of the network and change the number of strides to 1, such that the size of the feature map we obtained at CNN stage 4 is $2048 \times 24 \times 8$.

In all experiments, we set the size of parts as 6 and the margin in the triplet loss is 1.0 in our network. The size of mini-batch is 64 for each iteration. We use stochastic gradient descent (SGD) as the optimizer with a momentum of 0.9 and 0.0005 is the weight decay factor. We train our model for 150 epochs and set 0.01 as the initial learning rate, and later the warm-up learning rate as described in equal (6) is adopted. We follow the same experiments setting in all datasets.

The learning rate $lr(e)$ in epoch e is computed as:

$$lr(e) = \begin{cases} 3 \times 10^{-4} * \frac{e}{10}, & e \leq 10 \\ 0.01, & 10 < e \leq 60 \\ 0.005, & 60 < e \leq 90 \\ 0.0025, & 90 < e \leq 120 \\ 0.00125, & 120 < e \leq 150 \end{cases} \quad (6)$$

Evaluation metrics: To compare our method with existing advanced approaches, we use Cumulative Match Characteristics (CMC) and mean Average Precision (mAP) to measure their performances on all the datasets. Notably, we don't adopt the re-ranking strategy to improve the results in our experiments.

B. Datasets

Market-1501: This dataset includes 1,501 different identities of 32,668 images observed from six cameras with overlapping and one camera is low-resolution, five cameras

TABLE I

ALL DATASETS ARE FACED WITH SOME PRACTICAL CHALLENGES: DISAPPEARING SOME PARTS OF PERSON DUE TO OCCLUSIONS, CHANGES IN LIGHT AND VIEWPOINT, OR BOUNDING BOX ERRORS BECAUSE OF THE OBJECT DETECTORS. FOR THE CUHK03-NP DATASET, L MEANS MANUALLY LABELED BOUNDING BOXES, D MEANS DPM DETECTED.

Dataset	Market	Duke	CUHK03-NP (L/D)	MSMT17
Identities	1501	1812	1467	4101
Bounding boxes	32668	36411	13164	126441
Cameras	6	8	6	15
Label method	DMP/Hand	Hand	Hand/DPM	Faster RCNN
Train images	12936	16522	7368/7365	32621
Train ids	751	702	767	1041
Test images	19732	17661	5328/5332	93820
Test ids	750	702	700	3060

are high-resolution. Following the same setting in PCB [38], 751 IDs with 12,936 images are allocated for training and the rest 750 IDs with 19,732 gallery images and 3,368 query images building the testing set.

DukeMTMC-reID: This dataset consists of 1,404 identities, 2,228 queries, 17,661 gallery images, and 16,522 training images captured from 8 high-resolution cameras. The training set is randomly selected from 702 identities and the rest 702 pedestrians are utilized for testing. In addition, 408 additional dis-related identities are regarded as distractors.

CUHK03-NP: This dataset includes 14,097 images from 1,467 identities observed from 2 different cameras. There are two ways to obtain the annotations: manually labeled and DPM detected bounding boxes. For each camera, each person selects one image as the probe and we choose the rest images to construct the gallery set. The labelled dataset contains 767 identities, 7,368 training, 5,328 gallery and 1,400 query images while the detected set includes 767 identities, 7,365 training, 5,332 gallery and 1,400 query images.

MSMT17: It is a new person re-ID dataset, which includes 4,101 pedestrians and 126,441 bounding boxes. Different from other datasets, MSMT17 is randomly divided according to the ratio of training and testing 1:3. The training set includes 32,621 images with 1041 identities, while the testing set includes 93,820 images with 3060 identities.

Table I lists four datasets widely adopted in person re-ID task and some images are shown in Figure 6. All datasets contain many practical challenges, such as occlusions, changes in viewpoint and lighting, or misaligned bounding boxes from object detector.

C. Comparison with State-of-the-Art Approaches

We compare our model with some advanced approaches on four datasets in this section.

Market-1501: It is a standard dataset for person re-ID. Bounding boxes of probe images in the dataset are manually drawn, while pedestrian bounding boxes in gallery are detected by using DPM detector. Table II lists the results of our model and some advanced algorithms on Market-1501. From this table, we can find that our model obtains rank-1/mAP=95.7%/87.7% without using re-ranking algorithm. Table II presents the current main approaches and all of which integrate global and local features in their networks. As can be seen from this table, our method obtains the best performance on rank-1 and competitive result on mAP. GCP obtains the

TABLE II
COMPARISONS (%) ON MARKET-1501 AT 2 EVALUATION METRICS: MAP, RANK-1

Method	Backbone	Market-1501	
		Rank-1	mAP
DaRe (CVPR18) [33]	ResNet50	86.4	69.3
DaRe+RE (CVPR18) [33]	ResNet50	88.5	74.2
PSE+ECN (CVPR18) [36]	ResNet50	90.4	80.5
HA-CNN (CVPR18) [26]	ResNet50	91.2	75.7
DuATM (CVPR18) [37]	Inception-A	91.4	76.6
PCB+RPP (CVPR18) [38]	ResNet50	93.8	81.6
MHN-PCB (ICCV19) [45]	ResNet50	95.1	85.0
MGN (ACMMM18) [42]	ResNet50	95.7	86.9
HPM (AAAI19) [66]	ResNet50	94.2	82.7
AANet (CVPR19) [17]	ResNet152	93.9	83.4
DCDS(ICCV19) [46]	ResNet101	94.8	85.8
OSNet (ICCV19) [48]	OSNeT	94.8	84.9
GCP (AAAI20) [47]	ResNet50	94.8	88.0
SAN(AAAI20) [49]	ResNet50	95.1	85.8
3DTANet (TCSVT20) [50]	—	95.3	86.9
HOREID (CVPR20) [51]	ResNet50	94.2	84.9
RGA-CS(CVPR20) [52]	ResNet50	95.3	87.8
Ours	ResNet50	95.7	87.7

highest accuracy on mAP and only 0.3% improvement over our method.

DukeMTMC-reID: It is another standard dataset that contains a sufficient number of images for deep learning. Images in this dataset are of high quality and the pedestrian is complete. However, extra IDs are added to the dataset as a distraction for model training. The comparisons are reported in Table III. Our model also performs very well on this dataset and achieves rank-1=90.2%, mAP=80.2% accuracy, which outperform compared state-of-the-art algorithms by a large margin. Our model achieves the best results on mAP and Rank 1.

The top-10 ranking results of some queries are displayed in Figure 7. In this figure, the green bounding boxes list the correct match images and the red boxes list the wrong match images. The first three matching results show that our method has a strong robustness: the extracted features can identify the captured pedestrians well, regardless of their poses, views and lights changing. For the third query image, our method can still eliminate the interference of scene lighting changes to obtain accurate results. For the fourth query image, we can see that the current dataset contains a large number of similar images of pedestrians (ranks 1-10). Even with human eyes, it is impossible to distinguish whether these images belong to the same person, but our method can still obtain relatively



Fig. 7. Visualization results on DukeMTMC-reID dataset. The first column is probe images and the right part lists top-10 retrieved gallery images corresponding to the probe image (not from the same camera). The images with green bounding boxes are the true matches, and those with red boxes are false ones.

TABLE III
COMPARISONS (%) ON DUKMTMC-REID DATASET AT 2 EVALUATION
METRICS: MAP, RANK -1

Method	Backbone	DukeMTMC-ReID	
		Rank-1	mAP
SPReID (CVPR18) [53]	ResNet152	85.9	73.3
PCB+RPP (ECCV18) [38]	ResNet50	83.3	69.2
DuATM (CVPR18) [37]	DenseNet121	81.8	64.6
PSE+ECN(CVPR18) [36]	ResNet50	84.5	75.7
AANet (CVPR19) [17]	ResNet152	87.7	74.3
DCDS(ICCV19) [46]	ResNet101	87.6	75.5
CASN(CVPR19) [55]	ResNet50	87.7	73.7
HPM (AAAI19) [66]	ResNet50	86.6	74.3
MHN-PCB(ICCV19) [45]	ResNet50	89.1	77.2
OSNet (ICCV19) [48]	OSNET	88.6	73.5
MGN(ACMMM18) [42]	ResNet50	88.7	78.4
ABDNet (ICCV19) [56]	ResNet50	89.0	78.6
GCP(AAAI20) [47]	ResNet50	89.7	78.6
SAN(AAAI20) [49]	ResNet50	87.9	75.5
3DTANet (TCSVT20) [50]	—	89.9	78.4
M3+ ResNet50(CVPR20) [54]	ResNet50	84.7	68.5
M3+DenseNet121(CVPR20) [54]	DenseNet121	84.9	68.0
HOReID (CVPR20) [51]	ResNet50	86.9	75.6
Ours	ResNet50	90.2	80.2

accurate results (ranks 1-5).

CUHK03-NP: This is a challenging dataset. The challenge comes from the fact that it includes a large number of images with varied perspectives, pedestrian occlusions and low resolution which bring great interference to the training of the model.

However, the proposed method still obtains the best results and surpasses all competing algorithms on Rank 1. Our model also obtains the second best results on mAP. The comparisons are shown in Table IV. In our experiment, we adopt the new protocol of CUHK03 for training and testing. As can be seen when manually labeled bounding boxes are exploited, our method achieves Rank-1=80.3% and mAP=76.2% accuracy. When detected setting are used, our method obtains Rank-1=75.5% and mAP=72.5% accuracy.

MSMT17: This dataset is a new person re-ID dataset, which contains more pedestrians, more bounding boxes, and more cameras. It has more complex scenarios and backgrounds, such as outdoor and indoor. In addition, this dataset takes a long time to capture, covers multiple time periods, and has complex and obvious light changes. Faster RCNN, a better pedestrian detector was adopted to collect the dataset. Therefore, this dataset presents a more realistic situation, which is a great challenge for the current models. The comparison results with related methods are listed in Table V. Our approach obtains the Rank-1 of 79.6% and 57.6% on mAP, which is superior to most of related algorithms except ABDNet. Our model obtains the second best results on Rank-1 and mAP.

D. Ablation Study

To evaluate the usefulness of different components in our model, we perform several ablation experiments about each

TABLE IV

COMPARISON RESULTS (%) ON CUHK03 DATASET AT 2 EVALUATION METRICS: mAP, RANK-1. L REPRESENTS LABELED WHICH MEANS THAT THE PROBE IMAGES ARE LABELED BY HAND-CRAFTED. D REPRESENTS DETECTED WHICH MEANS THAT THE PROBE IMAGES ARE LABELED BY DPM.

Method	Backbone	CUHK03 (L)		CUHK03 (D)	
		Rank-1	mAP	Rank-1	mAP
DaRe (CVPR18) [33]	DenseNet121	56.4	52.2	54.3	50.1
Manacs (ECCV18) [58]	ResNet50	69.0	63.9	65.5	60.5
PCB+RPP(ECCV18) [38]	ResNet50	—	—	63.7	57.5
BFE(ICCV19) [57]	ResNet50	79.4	76.7	76.4	73.5
MGN (ACMMM18) [42]	ResNet50	68.0	67.4	66.8	66.0
MHN-PCB(ICCV19) [45]	ResNet50	77.2	72.4	71.7	65.4
HPM (AAAI19) [66]	ResNet50	—	—	63.1	57.5
OSNet (ICCV19) [48]	OSNET	72.3	67.8	—	—
CASN-PCB(CVPR19) [55]	ResNet50	73.7	68.0	71.5	64.4
M3+ResNet50(CVPR20) [54]	ResNet50	66.9	60.7	—	—
M3+DenseNet121(CVPR20) [54]	DenseNet121	61.6	54.4	—	—
GCP(AAAI20) [47]	ResNet50	77.9	75.6	77.9	69.6
3DTANet (TCSVT20) [50]	—	80.2	75.2	75.2	68.9
Ours	ResNet50	80.3	76.2	77.5	72.5

TABLE V

COMPARISONS (%) ON MSMT17 DATASET AT 3 EVALUATION METRICS: mAP, RANK-1 AND RANK-5.

Method	Backbone	MSMT17		
		Rank-1	Rank-5	mAP
GoogLeNet (ICCV17) [59]	GoogLeNet	47.6	—	23.0
PDC (ICCV17) [59]	GoogLeNet	58.0	73.6	29.7
GLAD (ACMMM17) [61]	ResNet50	61.4	76.8	34.0
IANet (CVPR19) [60]	ResNet50	75.5	85.5	46.8
BFE (ICCV19) [57]	ResNet50	78.8	89.1	51.5
ABDNet (ICCV19) [56]	ResNet50	82.3	90.6	60.8
OSNet (ICCV19) [48]	OSNET	78.7	—	52.9
SAN(AAAI20) [49]	ResNet50	79.2	—	55.7
3DTANet (TCSVT20) [50]	—	76.6	86.8	46.7
Circle Loss (CVPR20) [62]	ResNet50	76.3	—	50.2
Ours	ResNet50	79.6	90.2	57.6

TABLE VI

ABLATION STUDY ON DIFFERENT COMPONENTS IS EVALUATED ON MARKET 1501 AND DUKEMTMC-REID DATASETS.

Model	Market-1501		DukeMTMC-reID	
	Rank-1	mAP	Rank-1	mAP
Baseline	88.1	71.1	79.2	63.7
+ Bag of tricks	92.3	81.9	85.1	69.5
+ MPFE	93.4	83.4	86.6	73.5
+ MGO	94.7	86.5	88.6	77.9
+ SAM	95.3	87.2	89.2	78.1
+ CAM	95.7	87.7	90.2	80.2

component in a single query mode on Market-1501 dataset. Note that all the experiments in this section follow the same settings in Section IV. A.

Influences of Each Component (Same domain): Our network is composed of different components, so we add these components (SAM, CAM, MPFE, MGO and Bag of tricks) into the baseline in turn, and follow the same training settings. The ablation experiment can prove that each component plays a positive role in improving our model's performance.

The baseline we refer to in Section IV. A is ResNet-50, which can reach 71.1% and 88.1% of mAP and Rank 1 on the Market-1501 dataset. The performance of our baseline used can reach the same level compare with the baseline reported by other papers. Then we add Bag of tricks, MGO, MPFE, SAM and CAM to the baseline respectively during the

TABLE VII

ABLATION STUDY ON DIFFERENT COMPONENTS IS EVALUATED ON DUKEMTMC-REID DATASET.

Baseline	Tricks	MGO	MPFE	SAM	CAM	Rank-1	mAP
✓						79.2	63.7
✓	✓					85.1	69.5
✓		✓				84.9	69.5
✓			✓			83.6	71.2
✓				✓		84.3	72.3
✓					✓	85.1	72.8

training process. As shown in Table VI, the interaction of all these components makes our model reach 95.7% on Rank - 1 and 87.7% on mAP accuracy on Market-1501 dataset, and the individual experiment shows that each component has a positive effect for our model. Our approach has improved the baseline network by 7.6% of Rank-1 and 16.6% of mAP. It is noteworthy that in all the components, the use of local features can greatly improve our model's performance, especially the improvement effect of mAP.

Meanwhile, we also introduce different components into the baseline one by one to evaluate how framework components contribute to the baseline. We conducted multiple experiments on the DukeMTMC-reID dataset. As shown in Table VII, any single component can improve the performance of the model. This indicates that these five components are mutually complementary each other.

Influences of Each Component (Cross-domain): To further verify the usefulness of each of our components, we also perform cross-domain experiments and the results are listed in Table VIII below. To eliminate the negative effects caused by overfitting, cross-domain experiments are conducted on Market-1501 and DukeMTMC-reID datasets. Duke → Market means that train our model on DukeMTMC-reID dataset and evaluate it on Market-1501. Similarly, Market → Duke means that Market-1501 dataset is used for training and DukeMTMC-ReID is used for evaluating. From the results we can see that even in the cross-domain experiments, each of our components has positive impact on the performance. Especially, on Duke → Market, Bag of tricks and MGO have huge performance improvements from Rank-

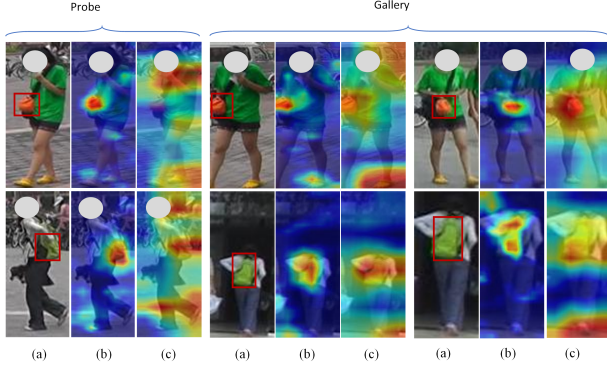


Fig. 8. Each triplet contains from left to right, (a) original image, (b) activation map of our model (Stage 4), and (c) activation map of baseline. These images show that our model is better able to focus on where is more discriminative feature.

1/mAP=33.43%/12.65% to 41.21%/17.13% (+7.78%/4.48%) and from Rank-1/mAP=42.31%/18.90% to 51.15%/24.68% (+8.84%/5.78%).

Effectiveness of Attention Module: As shown in Table IX, Baseline_{BMM} refers to adding Bag of Tricks, MGO and MPFE modules to the baseline and aims to verify the effect of attention module on the performance of our model. We use S and C to respectively represent spatial attention module (SAM) and channel attention module (CAM) and '⊙' represents connection operation. Therefore, S+C+⊙ means we first adopt CAM and then use SAM, finally perform connection operation. The character order represents the order in which operations are performed. Similarly, +S+C means the first step is to perform connection operation. C+⊙+S means the first step is to perform CAM. It can be seen from Table IX that Baseline_{BMM}+S+⊙+C can get the best results and achieves 95.7% on rank-1 and 87.7% on mAP accuracy. The second part of this Table shows the performance of our model after adding channel attention and spatial attention respectively (using the feature map of Stage 4 only). At the same time, we also consider the order of adding two attention modules into our model, which the results are shown in the third and fourth parts of this Table, respectively. We can see that when we first adopt spatial attention model and then perform connection, and finally adopt the channel attention model, our model can get the best results.

Fig. 8 displays the activation maps of different person images. This shows that our model can focus on more discriminative region than the baseline. We first look at the first row, it can be seen that our method can focus on the significant region, regardless of changes of the perspective. In addition, our method can also detect the same significant area with different perspectives and scales (the images in the second row).

The impact of multi-stage fusion: To evaluate the validity of the multi-level fusion, we divide our model into different stages and judge the validity of our model by fusing different stages of features. Table X lists the results our model at different stages, trained with random erasing and evaluated without re-ranking algorithm. By comparing the results of

TABLE VIII
ABLATION STUDY ON DIFFERENT COMPONENTS IS EVALUATED ON CROSS-DOMAIN DATASETS. DUKE → MARKET MEANS TRAINED ON DUKE-MTMC-REID AND EVALUATED IT ON MARKET-1501.

Model	Duke → Market		Market → Duke	
	Rank-1	mAP	Rank-1	mAP
Baseline	33.43	12.65	19.61	9.19
+ Bag of tricks	41.21	17.13	30.48	15.95
+ MPFE	42.31	18.90	34.07	18.22
+ MGO	51.15	24.68	39.86	23.01
+ SAM	51.98	25.16	40.79	23.96
+ CAM	54.33	26.43	42.52	25.37

TABLE IX
THE PERFORMANCE OF ATTENTION MODULE IS EVALUATED ON MARKET1501 DATASETS.

Model	Rank-1	mAP
Baseline _{BMM}	94.7	86.5
Baseline _{BMM} + S	94.9	86.6
Baseline _{BMM} + C	95.1	86.9
Baseline _{BMM} + ⊙+C+S	94.8	86.7
Baseline _{BMM} + C+S+⊙	95.3	86.2
Baseline _{BMM} + C+⊙+S	95.3	87.2
Baseline _{BMM} + ⊙+S+C	95.0	86.9
Baseline _{BMM} + S+C+⊙	95.5	87.2
Baseline _{BMM} + S+⊙+C	95.7	87.7

TABLE X
RESULTS (%) WITH MULTI STAGES ON MARKET-1501 AND DUKE-MTMC-REID DATASETS.

Model	Market-1501		DukeMTMC-reID	
	Rank-1	mAP	Rank-1	mAP
stage 1	84.80	63.67	74.69	55.67
stage 2	90.62	76.02	82.50	67.56
stage 3	93.89	83.43	87.93	75.36
stage 4	93.72	86.05	88.63	77.47
stage 1-2	90.80	76.06	82.23	68.00
stage 1-3	94.42	85.85	88.33	76.09
stage 2-4	95.24	86.93	88.78	78.01
All stage	95.65	87.67	90.17	80.16

different stages, we can observe that as the stages gradually increase, the performance of our network gradually improves from rank-1/mAP= 84.80/63.67% to 95.65/87.67%. In addition, we also see that if we only consider single stage, with the increase number of stages, deeper convolutional network can extract more discriminative features. However, note that stage 3 achieves higher performance than stage 4. The possible reason is that in stage 4, the features are too high level and too much information will be lost because of the extra pooling layers. As expected, the fusion of all the stages can get the best results, and mAP also gains a lot of improvements. This indicates that the robustness of the features after fusion has been greatly improved. Whats more, it is also worth noting that even if we only fuse a few stages of features such as stages 1-2, stages 1-3 and stages 2-4, our results still exceed most of related algorithms.

V. CONCLUSION

In this paper, we proposed a novel deeply supervised model for addressing the challenging person re-ID problem. By fusing the the low- and high-level of feature maps from any network, our model can effectively reduce the information

loss. Our model can directly learn different granularity of local features from different stages, which are not used in some part locating operations such as pose information. Hybrid-attention mechanisms are also introduced into our model to obtain more valuable features at spatial and channel levels. Finally, We adopted two loss functions to train the network and learned the discriminative features for improving the matching performance. Experimental results display that our approach is superior to many state-of-the-art approaches.

REFERENCES

- [1] F. Michela, B. Loris, P. Alessandro, M. Vittorio and C. Marco, "Person re-identification by symmetry-driven accumulation of local features," in *Proc. IEEE Conf. Comput. Vis. Pattern Recognit.*, 2010, pp. 2360-2367.
- [2] D. Gray, and H. Tao, "Viewpoint invariant pedestrian recognition with an ensemble of localized features," in *Proc. Eur. Conf. Comput. Vis.*, 2008, pp. 262-275.
- [3] I. Kviatkovsky, A. Adam, and E. Rivlin, "Color invariants for person reidentification," *IEEE Trans. Pattern Anal. Mach. Intell.*, vol. 35, no. 7, pp. 1622-1634, 2012.
- [4] S. Liao, Y. Hu, X. Zhu, and S. Li, "Person re-identification by local maximal occurrence representation and metric learning," in *Proc. IEEE Conf. Comput. Vis. Pattern Recognit.*, 2015, pp. 2197-2206.
- [5] B. Ma, Su Y, and Jurie F, "Local descriptors encoded by fisher vectors for person re-identification," in *Proc. Eur. Conf. Comput. Vis.*, 2012, pp. 413-422.
- [6] S. Bai, X. Bai, and Q. Tian, "Scalable person re-identification on supervised smoothed manifold," in *Proc. IEEE Conf. Comput. Vis. Pattern Recognit.*, 2017, pp. 2530-2539.
- [7] M. Dikmen, E. Akbas, T. S. Huang, and N. Ahuja, "Pedestrian recognition with a learned metric," in *Proc. Asian Conf. Comput. Vis.*, 2010, pp. 501-512.
- [8] Z. Zhong, L. Zheng, Z. Zheng, S. Li, and Y. Yang, "CamStyle: a novel data augmentation method for person re-identification," vol. 28, no. 3, pp. 1176-1190, 2019.
- [9] E. Ahmed, M. Jones, and T. K. Marks, "An improved deep learning architecture for person re-identification," in *Proc. IEEE Conf. Comput. Vis. Pattern Recognit.*, 2015, pp. 3908-3916.
- [10] W. Deng, L. Zheng, Q. Ye, G. Kang, Y. Yang, and J. Jiao, "Image-image domain adaptation with preserved self-similarity and domain-dissimilarity for person re-identification," in *Proc. IEEE Conf. Comput. Vis. Pattern Recognit.*, 2018, pp. 994-1003.
- [11] Y. Huang, J. Xu, Q. Wu, Z. Zheng, Z. Zhang, and J. Zhang, "Multi-pseudo regularized label for generated data in person re-identification," *IEEE Trans. Image Process.*, vol. 28, no. 3, pp. 1391-1403, 2018.
- [12] X. Qian, Y. Fu, T. Xiang, W. Wang, J. Qiu, Y. Wu, Y. Jiang, and X. Xue, "Pose-normalized image generation for person re-identification," in *Proc. Eur. Conf. Comput. Vis.*, 2018, pp. 650-667.
- [13] Z. Zhong, L. Zheng, Z. Zheng, S. Li, and Y. Yang, "Camera style adaptation for person re-identification," in *Proc. IEEE Conf. Comput. Vis. Pattern Recognit.*, 2018, pp. 5157-5166.
- [14] X. Chen, Y. Duan, R. Houthoofd, J. Schulman, I. Sutskever, and P. Abbeel, "Infogan: Interpretable representation learning by information maximizing generative adversarial nets," *Advances in neural information processing systems.*, 2016, pp. 2172-2180.
- [15] L. Ma, Q. Sun, S. Georgoulis, G. L. Van, B. Schiele, and M. Fritz, "Disentangled person image generation," in *Proc. IEEE Conf. Comput. Vis. Pattern Recognit.*, 2018, pp. 99-108.
- [16] J. Xu, R. Zhao, F. Zhu, H. Wang, W. Ouyang, "Attention-aware compositional network for person re-identification," in *Proc. IEEE Conf. Comput. Vis. Pattern Recognit.*, 2018, pp. 2119-2128.
- [17] C. P. Tay, S. Roy, and K. H. Yap, "AANet: Attribute Attention Network for Person Re-Identifications," in *Proc. IEEE Conf. Comput. Vis. Pattern Recognit.*, 2019, pp. 7134-7143.
- [18] L. Zheng, Y. Yang, and A. G. Hauptmann, "Person re-identification: Past, present and future," *arXiv preprint arXiv:1610.02984*, 2016.
- [19] Z. Zheng, L. Zheng, and Y. Yang, "Unlabeled samples generated by gan improve the person re-identification baseline in vitro," in *Proc. IEEE Int. Conf. Comput. Vis.*, 2017, pp. 3754-3762.
- [20] G. Liang, X. Lan, X. Chen, K. Zheng, S. Wang, and N. Zhang, "Cross-view person identification based on confidence-weighted human pose matching," vol. 28, no. 8, pp. 3821-3835, 2019.
- [21] Z. Zheng, L. Zheng, and Y. Yang, "Pedestrian alignment network for large-scale person re-identification," *IEEE Trans. Circuits Syst. Video Technol.*, vol. 29, no. 10, pp. 3037-3045, 2018.
- [22] Y. Sun, L. Zheng, W. Deng, and S. Wang, "Svdnet for pedestrian retrieval," in *Proc. IEEE Int. Conf. Comput. Vis.*, 2017, pp. 3800-3808.
- [23] A. Hermans, L. Beyer, and B. Leibe, "In defense of the triplet loss for person re-identification," *arXiv preprint arXiv:1703.07737*, 2017.
- [24] X. Chang, T. M. Hospedales, and T. Xiang, "Multi-level factorisation net for person re-identification," in *Proc. IEEE Conf. Comput. Vis. Pattern Recognit.*, 2018, pp. 2109-2118.
- [25] X. Liu, H. Zhao, M. Tian, L. Sheng, J. Shao, S. Yi, J. Yan, and X. Wang, "Hydraplus-net: Attentive deep features for pedestrian analysis," in *Proc. IEEE Int. Conf. Comput. Vis.*, 2017, pp. 350-359.
- [26] W. Li, X. Zhu, and S. Gong, "Harmonious attention network for person re-identification," in *Proc. IEEE Conf. Comput. Vis. Pattern Recognit.*, 2018, pp. 2285-2294.
- [27] Y. Sun, Q. Xu, Y. Li, C. Zhang, Y. Li, S. Wang, and J. Sun, "Perceive where to focus: learning visibility-aware part-level features for partial person re-identification," in *Proc. IEEE Conf. Comput. Vis. Pattern Recognit.*, 2019, pp. 393-402.
- [28] C. Farabet, C. Couprie, L. Najman, and Y. LeCun, "Learning hierarchical features for scene labeling," *IEEE Trans. Pattern Anal. Mach. Intell.*, vol. 35, no. 8, pp. 1915-1929, 2012.
- [29] B. Hariharan, P. Arbeláez, R. Girshick, and J. Malik, "Hypercolumns for object segmentation and fine-grained localization," in *Proc. IEEE Conf. Comput. Vis. Pattern Recognit.*, 2015, pp. 447-456.
- [30] J. Long, E. Shelhamer, and T. Darrell, "Fully convolutional networks for semantic segmentation," in *Proc. IEEE Conf. Comput. Vis. Pattern Recognit.*, 2015, pp. 3431-3440.
- [31] T. Y. Lin, P. Dollár, R. Girshick, K. He, B. Hariharan, and S. Belongie, "Feature pyramid networks for object detection," in *Proc. IEEE Conf. Comput. Vis. Pattern Recognit.*, 2017, pp. 2117-2125.
- [32] S. Xie, Z. Tu, "Holistically-nested edge detection," in *Proc. IEEE Int. Conf. Comput. Vis.*, 2015, pp. 1395-1403.
- [33] Y. Wang, L. Wang, Y. You, X. Zou, Y. Chen, S. Li, G. Huang, B. Hariharan, and K. Q. Weinberger, "Resource aware person re-identification across multiple resolutions," in *Proc. IEEE Conf. Comput. Vis. Pattern Recognit.*, 2018, pp. 8042-8051.
- [34] L. Zheng, L. Shen, L. Tian, S. Wang, J. Wang, and Q. Tian, "Scalable person re-identification: A benchmark," in *Proc. IEEE Int. Conf. Comput. Vis.*, 2015, pp. 1116-1124.
- [35] W. Li, R. Zhao, T. Xiao, and X. Wang, "Deepreid: Deep filter pairing neural network for person re-identification," in *Proc. IEEE Conf. Comput. Vis. Pattern Recognit.*, 2014, pp. 152-159.
- [36] S. M. Saquib, A. Schumann, A. Eberle, and R. Stiefelhagen, "A pose-sensitive embedding for person re-identification with expanded cross neighborhood re-ranking," in *Proc. IEEE Conf. Comput. Vis. Pattern Recognit.*, 2018, pp. 420-429.
- [37] J. Si, H. Zhang, C. G. Li, J. Kuen, X. Kong, A. C. Kot, and G. Wang, "Dual attention matching network for context-aware feature sequence based person re-identification," in *Proc. IEEE Conf. Comput. Vis. Pattern Recognit.*, 2018, pp. 5363-5372.
- [38] Y. Sun, L. Zheng, Y. Yang, Q. Tian and S. Wang, "Beyond part models: Person retrieval with refined part pooling (and a strong convolutional baseline)," in *Proc. Eur. Conf. Comput. Vis.*, 2018, pp. 480-496.
- [39] H. Huang, D. Li, Z. Zhang, X. Chen, and K. Huang, "Adversarially occluded samples for person re-identification," in *Proc. IEEE Conf. Comput. Vis. Pattern Recognit.*, 2018, pp. 5098-5107.
- [40] D. Chen, D. Xu, H. Li, N. Sebe, and X. Wang, "Group consistent similarity learning via deep crf for person re-identification," in *Proc. IEEE Conf. Comput. Vis. Pattern Recognit.*, 2018, pp. 8649-8658.
- [41] J. Almazan, B. Gajic, N. Murray, and D. Larlus, "Re-id done right: towards good practices for person re-identification," *arXiv preprint arXiv:1801.05339*, 2018.
- [42] G. Wang, Y. Yuan, X. Chen, J. Li, and X. Zhou, "Learning discriminative features with multiple granularities for person re-identification," in *Proc. ACM Int. Conf. Multimedia.*, 2018, pp. 274-282.
- [43] M. Zheng, S. Karanam, Z. Wu, and R. J. Radke, "Re-Identification with Consistent Attentive Siamese Networks," in *Proc. IEEE Conf. Comput. Vis. Pattern Recognit.*, 2019, pp. 5735-5744.
- [44] X. Sun, and L. Zheng, "Dissecting person re-identification from the viewpoint of viewpoint," in *Proc. IEEE Conf. Comput. Vis. Pattern Recognit.*, 2019, pp. 608-617.
- [45] B. Chen, W. Deng, and J. Hu, "Mixed high-order attention network for person re-identification," in *Proc. IEEE Int. Conf. Comput. Vis.*, 2019, pp. 371-381.

- [46] L. T. Alemu, M. Pelillo, and M. Shah, "Deep constrained dominant sets for person re-identification," in *Proc. IEEE Conf. Comput. Vis. Pattern Recognit.*, 2019, pp. 9855-9864.
- [47] H. Park, and B. Ham, "Relation Network for Person Re-identification," *arXiv preprint arXiv:1911.09318*, 2019.
- [48] K. Zhou, Y. Yang, A. Cavallaro, and T. Xiang, "Omni-scale feature learning for person re-identification," in *Proc. IEEE Conf. Comput. Vis. Pattern Recognit.*, 2019, pp. 3702-3712.
- [49] X. Jin, C. Lan, W. Zeng, W. G. Wei, and Z. Chen, "Semantics-Aligned Representation Learning for Person Re-Identification," in *Proc. AAAI Conf. Artif. Intell.*, 2020, pp. 11173-11180.
- [50] Y. Huang, S. Lian, S. Zhang, H. Hu, D. Chen, and T. Su, "Three-Dimension Transmissible Attention Network for Person Re-Identification," *IEEE Trans. Circuits Syst. Video Technol.*, 2020.
- [51] Y. Ge, D. Chen, F. Zhu, R. Zhao, and H. Li, "Self-paced Contrastive Learning with Hybrid Memory for Domain Adaptive Object Re-ID," *arXiv preprint arXiv:2006.02713*, 2020.
- [52] Z. Zhang, C. Lan, W. Zeng, X. Jin, and Z. Chen, "Relation-Aware Global Attention for Person Re-identification," in *Proc. IEEE Conf. Comput. Vis. Pattern Recognit.*, 2020, pp. 3186-3195.
- [53] M. M. Kalayeh, E. Basaran, M. Gokmen, M. E. Kamasak, and M. Shah, "Human semantic parsing for person re-identification," in *Proc. IEEE Conf. Comput. Vis. Pattern Recognit.*, 2018, pp. 1062-1071.
- [54] J. Zhou, B. Su, and Y. Wu, "Online Joint Multi-Metric Adaptation from Frequent Sharing-Subset Mining for Person Re-Identification," in *Proc. IEEE Conf. Comput. Vis. Pattern Recognit.*, 2020, pp. 2909-2918.
- [55] M. Zheng, S. Karanam, Z. Wu, and R. J. Radke, "Re-identification with consistent attentive siamese networks," in *Proc. IEEE Conf. Comput. Vis. Pattern Recognit.*, 2019, pp. 5735-5744.
- [56] T. Chen, S. Ding, J. Xie, Y. Yuan, W. Chen, Y. Yang, Z. Ren, and Z. Wang, "Abdnet: Attentive but diverse person re-identification," in *Proc. IEEE Int. Conf. Comput. Vis.*, 2019, pp. 8351-8361.
- [57] Z. Dai, M. Chen, X. Gu, S. Zhu, and P. Tan, "Batch dropblock network for person reidentification and beyond," in *Proc. IEEE Int. Conf. Comput. Vis.*, 2019, pp. 3691-3701.
- [58] C. Wang, Q. Zhang, C. Huang, W. Liu, and X. Wang, "Manacs: A multi-task attentional network with curriculum sampling for person re-identification," in *Proc. Eur. Conf. Comput. Vis.*, 2018, pp. 365-381.
- [59] C. Su, J. Li, S. Zhang, J. Xing, W. Gao, and Q. Tian, "Pose-driven deep convolutional model for person re-identification," in *Proc. IEEE Int. Conf. Comput. Vis.*, 2017, pp. 3960-3969.
- [60] R. Hou, B. Ma, H. Chang, X. Gu, S. Shan, and X. Chen, "Interaction-and-aggregation network for person re-identification," in *Proc. IEEE Conf. Comput. Vis. Pattern Recognit.*, 2019, pp. 9317-9326.
- [61] L. Wei, S. Zhang, H. Yao, W. Gao, and Q. Tian, "Glad: Global-local-alignment descriptor for pedestrian retrieval," in *Proc. ACM Int. Conf. Multimedia.*, 2017, pp. 420-428.
- [62] Y. Sun, C. Cheng, Y. Zhang, C. Zhang, L. Zheng, Z. Wang, and Y. Wei, "Circle loss: A unified perspective of pair similarity optimization," in *Proc. IEEE Conf. Comput. Vis. Pattern Recognit.*, 2020, pp. 6398-6407.
- [63] X. Chang, T. M. Hospedales, T. Xiang, "Multi-level factorisation net for person re-identification," in *Proc. IEEE Conf. Comput. Vis. Pattern Recognit.*, 2018, pp. 2109-2118.
- [64] S. Woo, J. Park, J. Y. Lee, I. S. Kweon, "Cbam: Convolutional block attention module," in *Proc. Eur. Conf. Comput. Vis.*, 2018, pp. 3-19.
- [65] L. Wei, S. Zhang, W. Gao, and Q. Tian, "Person transfer gan to bridge domain gap for person re-identification" in *Proc. IEEE Conf. Comput. Vis. Pattern Recognit.*, 2018, pp. 79-88.
- [66] Fu Y, Wei Y, Zhou Y, et al. "Horizontal Pyramid Matching for Person Re-identification" in *Proc. AAAI Conf. Artif. Intell.*, 2019, pp. 8295-8302.